Linear-Quadratic Gaussian with Loop-Transfer Recovery Methodology for the F-100 Engine

Michael Athans,* Petros Kapasouris,† Efthimios Kappos,‡ and H.A. Spang III§
Massachusetts Institute of Technology, Cambridge, Massachusetts

The design of a multivariable feedback control system for the F-100 turbofan jet engine is a challenging task for control engineers. This paper employs a linearized model of the F-100 engine to demonstrate the use of the newly developed linear-quadratic Gaussian with loop-transfer recovery design methodology that adopts an integrated frequency and time-domain approach to multivariable feedback control synthesis so as to meet stability robustness, command following, and disturbance rejection specifications.

Introduction

MODERN turbofan jet engines represent an important multiple-input/multiple-output (MIMO) control application area since the dynamic coordination of fuel flow and several engine geometry variables can lead to improved performance and efficiency, while maintaining safe fan and compression stall margins. Indeed, the MIMO feedback control of turbofan and turboshaft engine has received a great deal of attention in the past few years.[1-8]

The F-100 turbofan engine was used as a main design example for which different MIMO control methodologies were employed. The so-called linear-quadratic-regulator (LQR) approach[9,10] was the basis of engineering designs and evaluations[1-4] that required the feedback of several F-100 state variables.

In the past five years significant advances have been made in integrating time-domain optimization-based approaches [such as LQR and linear-quadratic Gaussian (LQG)] with frequency domain approaches. Such an integrated frequency-domain and state-space approach to MIMO control systems design was pioneered by Stein and his colleagues[11-14] and has culminated to the so-called linear-quadratic Gaussian with loop-transfer recovery (LQG/LTR) methodology for MIMO feedback control synthesis.

The primary objective of this paper is to illustrate the LQG/LTR design methodology using a four-input/four-output linear model of the F-100 engine. Specifically, we stress how MIMO command following and disturbance rejection performance specifications, as well as stability robustness specifications are naturally posed in the frequency domain using the singular values of suitably defined loop-transfer matrices. Then, we demonstrate how the LQG/LTR design procedure is used to meet the posed specifications. Furthermore, we exploit the MIMO residue (or partial fraction) expansion method to reduce both the dimensionality of the design model and of the dynamic compensator.

The LQG/LTR methodology[11-14] requires direct measurement of only the output variables that must be independently controlled to meet the posed command following and disturbance rejection specifications. As such, it represents a significant departure from traditional LQR and LQG optimal control methodologies,[9,10] which may require the real-time measurement of several more variables. Hence, the resultant LQG/LTR based design is significantly different from those documented in the open literature for the F-100 engine.[1-4] Specifically, more attention is given to the stability robustness issue[15,16] of modeling errors.

Submitted June 21, 1984; presented as Paper 84-1910 at the AIAA Guidance and Control Conference, Seattle, WA, Aug. 20-22, 1984; revision received Feb. 4, 1985.

*Professor, Department of Electrical Engineering and Computer Science, Laboratory for Information and Design System. Member AIAA.

†Graduate Student, Department of Electrical Engineering and Computer Science, Laboratory for Information and Design System.

‡Graduate Student (currently at University of California, Berkeley).

§Adjunct Professor, Department of Electrical Engineering and Computer Science, Laboratory for Information and Design System. (Also with General Electric Company Corporate Research and Development Center, Schenectady, NY.)

The F-100 Linear Model

The Engine, Actuator, and Sensor Dynamics

The development of the control system will be based on the linear model of the F-100 jet engine,[1-4] which is an approximation of the engine dynamics at the operating point of 83 deg power level angle, sea level, static.

The linear model of the F-100 jet engine includes 16 state variables (Table 1), 4 control variables (Table 2), and 4 output variables (Table 3). To make the linear model more accurate, the dynamics of the control actuators and of the fan turbine inlet temperature sensor are also included. So the "truth" model of the engine contains 23 state variables, 4 controls, and 4 outputs.

Table 4 shows the open-loop eigenvalues (poles) and the transmission zeros of the four-input/four output F-100 truth model. Note the wide spread of the open-loop poles (-0.18204 to -577.04 rad/s).

Bandwidth Specifications

Figure 1 shows the closed-loop configuration of the MIMO feedback control system including the linear compensator to be designed $[\boldsymbol{K}(s)]$. From Fig. 1, the following equation can be derived:

$$\boldsymbol{y}(s) = \boldsymbol{G}(s)\boldsymbol{K}(s)[\boldsymbol{I}+\boldsymbol{G}(s)\boldsymbol{K}(s)]^{-1}\boldsymbol{r}(s) + [\boldsymbol{I}+\boldsymbol{G}(s)\boldsymbol{K}(s)]^{-1}\boldsymbol{d}(s) \quad (1)$$

Equation (1) suggests that in order to have "good" command following and "good" disturbance rejection, the loop-transfer function matrix (LTFM) $[\boldsymbol{G}(s)\boldsymbol{K}(s)]$ has to be "large" and, consequently, the minimum singular value $\sigma_{\min}[\boldsymbol{G}(j\omega)\boldsymbol{K}(j\omega)]$ should be "large" in the appropriate frequency regions.

Also, for "good" sensor noise rejection and robust design (stable in the presence of high-frequency modeling uncertainties), the LTFM $[\boldsymbol{G}(s)\boldsymbol{K}(s)]$ has to be "small" and, consequently, $\sigma_{\max}[\boldsymbol{G}(j\omega)\boldsymbol{K}(j\omega)]$ must be "small" in the appropriate frequency regions. Commands and disturbances have to dominate in frequency regions different from the noises and modeling errors for all of the constraints to be satisfied.

In accordance with the control specifications,[4] all of the settling times are required to be around 2-3 s, which means that the minimum crossover frequency has to be around 2 rad/s. Taking into account the robustness requirement [see Eq. (37)], the maximum allowable crossover frequency is about 10 rad/s. Also, a tight crossover pattern for the LTFM singular values is desirable, so that the different loops have approximately the same speed of response. Another performance requirement is to have a zero steady-state error rate for the step command inputs and/or step distrubances in any channel; thus, an integrator is required in each control channel.

These constraints are noted graphically in Fig. 5 where the shaded areas indicate the regions to be avoided. The curves shown in Fig. 5 are the open-loop frequency response resulting from the LQG/LTR design procedure.

Model Reduction

The truth model of the F-100 jet engine includes 23 state variables. One can design a four-input/four-output LQG/LTR compensator $[\boldsymbol{K}(s)]$ for this model to meet the specifications. The resultant MIMO compensator will then have 31 states (23+4+4), since 4 integrators have to be added to the truth model to meet the zero steady-state error requirement for the step command and disturbance inputs.

Since the crossover frequency requirement is about 10 rad/s and since the truth model includes poles in the order of 577 rad/s, one may conjecture that, if a compensator is carefully designed for a reduced-order linear model, it will "work" for the "truth" model. The model approximation idea is to preserve all of the important modes of the "truth" model in the low-frequency region.

The neglected dynamics will be taken care of in the description of the modeling uncertainty. The stability robustness of the reduced-order design will be guaranteed by singular value inequalities.[11-16]

MIMO Residue Method for Model Reduction

The MIMO residue method, although neglected in the literature, offers a straightforward and powerful method for model simplification. The idea behind the MIMO residual method is simple and is outlined here.

Consider the state-space description of a "square" linear time-invariant system with the same number of inputs and outputs,

$$\dot{\boldsymbol{x}}(t)=\boldsymbol{A}\boldsymbol{x}(t)+\boldsymbol{B}\boldsymbol{u}(t), \qquad \boldsymbol{y}(t)=\boldsymbol{C}\boldsymbol{x}(t) \tag{2}$$

with $\boldsymbol{x}(t)\in R^n$, $\boldsymbol{u}(t)\in R^p$ and $\boldsymbol{y}(t)\in R^p$.

Let λ_i $(i=1,2,\ldots,n)$ be the distinct eigenvalues of $\boldsymbol{A}$, $\boldsymbol{u}_i$ the corresponding right eigenvector (column vector), and $\boldsymbol{v}_i^T$ the corresponding left eigenvector (row vector). Thus, for $i=1,2,\ldots,n$,

$$\boldsymbol{A}\boldsymbol{u}_i=\lambda_i\boldsymbol{u}_i; \qquad \boldsymbol{v}^T\boldsymbol{A}=\lambda_i\boldsymbol{v}_i^T \tag{3}$$

In the frequency domain, the system of Eq. (2) is represented by the $p\times p$ transfer function matrix $\boldsymbol{G}(s)$ so that

$$\boldsymbol{y}(s)=\boldsymbol{G}(s)\boldsymbol{u}(s) \tag{4}$$

where

$$\boldsymbol{G}(s)=\boldsymbol{C}(s\boldsymbol{I}-\boldsymbol{A})^{-1}\boldsymbol{B} \tag{5}$$

Under the assumption of distinct eigenvalues [poles of $\boldsymbol{G}(s)$], the MIMO partial fraction expansion is

$$\boldsymbol{G}(s)=\sum_{i=1}^{n}\frac{\boldsymbol{R}_i}{s-\lambda_i}=\sum_{i=1}^{n}\frac{\boldsymbol{R}_i/\lambda_i}{(s/\lambda_i)-1} \tag{6}$$

The $p\times p$ (complex-valued) matrix $\boldsymbol{R}_i$ is called the residue matrix at pole $s=\lambda_i$, $i=1,2,\ldots,n$. The residue matrices can be readily calculated from the time-domain description [Eq. (2)] and the left and right eigenvectors defined in Eq. (3) as follows:

$$\boldsymbol{R}_i=\boldsymbol{C}\boldsymbol{u}_i\boldsymbol{v}_i^T\boldsymbol{B} \tag{7}$$

For $s=j\omega$, Eq. (6) reduces to

$$\boldsymbol{G}(j\omega)=\sum_{i=1}^{n}\frac{\boldsymbol{R}_i/\lambda_i}{(j\omega/\lambda_i)-1} \tag{8}$$

Table 1 Engine states

x_1 = fan speed $N1$, rpm
x_2 = compressor speed $N2$, rpm
x_3 = compressor discharge pressure P_{t3}, psia
x_4 = interturbine volume pressure $P_{t4.5}$, psia
x_5 = augmentor pressure P_{t7} psia
x_6 = fan discharge temperature $T_{t2.5}$, °R
x_7 = duct temperature $T_{t2,5lo}$, °R
x_8 = compressor discharge temperature T_{t3}, °R
x_9 = burner exit fast response temperature T_{t4hi}, °R
x_{10} = burner exit slow response temperature T_{t4lo} – °R
x_{11} = burner exit total temperature T_{t4}, °R
x_{12} = fan turbine inlet fast temperature $T_{t4.5hi}$, °R
x_{13} = fan turbine inlet slow temperature $T_{t4.5lo}$, °R
x_{14} = fan turbine exit temperature T_{t5}, °R
x_{15} = duct exit temperature T_{t6}, °R
x_{16} = duct exit temperature T_{t7}, °R

Table 2 Engine control inputs

u_1 = main burner fuel flow WFMB, lb/h
u_2 = exit nozzle area A_j, ft^2
u_3 = inlet guide vane position VG_1, deg
u_4 = high variable stator position VG_2, deg

Table 3 Engine outputs

$y_1=x_1$ = fan speed
$y_2=x_2$ = compressor speed
$y_3=x_3$ = compressor discharge pressure
$y_4=x_{12}+x_{13}$ = fan turbine inlet temperature

Table 4 Engine, actuator, and sensor poles and zeros

Poles		Zeros
1) −0.182	13) −21.+j31.3	1) −0.47
2) −0.648	14) −21.−j31.3	2) −0.649
3) −1.68	15) −21.3+j0.8	3) −2.13
4) −1.91	16) −21.3−j0.8	4) −19.47
5) −2.62	17) −38.68	5) −20.0
6) −6.7+j1.3	18) −40.	6) −20.9
7) −6.7+j1.3	19) −47.13	
8) −10.	20) −50.67	
9) −12.	21) −59.2	
10) −17.8+j4.8	22) −175.7	
11) −17.8−j4.8	23) −577.0	
12) −18.6		

The magnitude of each residue matrix provides a measure of the importance of the contribution of the corresponding pole in the MIMO input/output system description. The choice of the poles to be retained and the poles to be neglected should be made in accordance of the magnitude of the residue matrix *and* of the pole location (frequency) relative to the bandwidth specifications. For example, a pole that has a "large" residue matrix may be neglected if its frequency is much higher than the desired crossover frequency. A pole within the desired bandwidth may also be neglected provided that its residue matrix is "small," a characteristic of approximate MIMO pole-zero cancellation.

A step-by-step model reduction method will be presented and will be used for the reduction of the linear F-100 model and later of the LQG/LTR compensator. Assume that the reduced model $G_r(s)$ or order r is of the form

$$\dot{z}(t) = Fz(t) + Gu(t) \tag{9}$$

$$y(t) = Hz(t) + Du(t) \tag{10}$$

with $z(t) \in R^r$, $u(t) \in R^p$, $y(t) \in R^p$, $r > n$, and

$$z(t) = Kx(t) \tag{11}$$

where K is an $r \times n$ constant matrix. Note that the physical significance and dimensions of the control $u(t)$ and output $y(t)$ have been retained. The model reduction method is as follows:

1) Write the system transfer function matrix in the residue matrix sum as in Eq. (8) and find the magnitude of the residue matrices (any norm can be used). According to the crossover specifications and the magnitude of the residues, *decide which poles will be eliminated.* Suppose that the reduced model has as eigenvalues the subset of the A matrix eigenvalues $[\lambda_1(A),\ldots,\lambda_r(A)]$, suitably arranged.

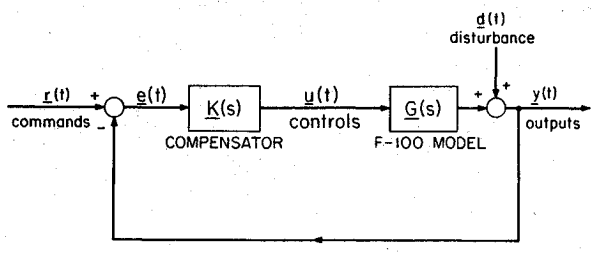

Fig. 1 MIMO closed-loop system.

2) Define the matrix

$$T = \begin{bmatrix} T_1 & & 0 \\ & \ddots & \\ 0 & & T_j \end{bmatrix} \tag{12}$$

where

$T_k = 1$ for each distinct real eigenvalue that is retained

$$T_k = \begin{bmatrix} \frac{1}{2} & -j/2 \\ \frac{1}{2} & j/2 \end{bmatrix}$$ for each complex pair of eigenvalues retained

and

$$\sum_{k=1}^{j} \dim(T_k) = r$$

3) Calculate the matrix K in Eq. (11) by

$$K \triangleq (T)^{-1} \begin{bmatrix} v_1^T \\ \vdots \\ v_r^T \end{bmatrix} \tag{13}$$

and the matrix M by

$$M \triangleq (u_1,\ldots,u_r)T \tag{14}$$

with the u_i and v_j defined in Eq. (3).

4) The matrices in the reduced-state space model [Eqs. (9) and (10)] are computed by

$$F = KAM \tag{15}$$

$$G = KB \tag{16}$$

$$H = CM \tag{17}$$

$$D = \sum_{i=r+1}^{n} \frac{R_i}{(-\lambda_i)} \tag{18}$$

where $(\lambda_{r+1},\ldots,\lambda_n)$ are the neglected eigenvalues. Note that the transfer function of the reduced model $G_r(s)$, given by

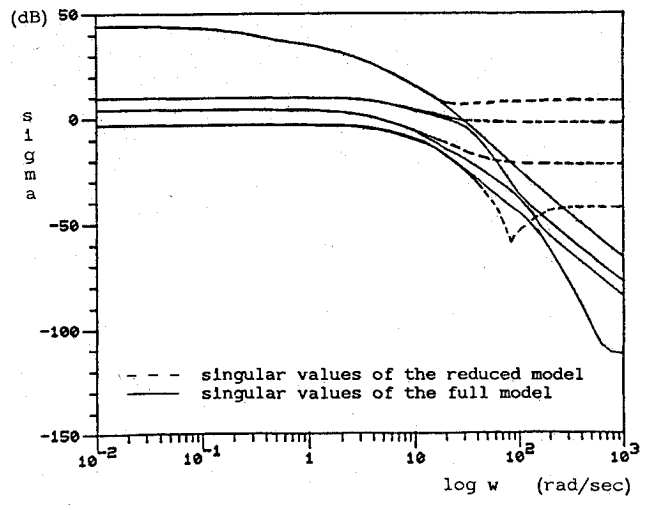

Fig. 2 Singular values of the scaled F-100 truth model (23 states) $G(s)$ and the singular values of the reduced F-100 model (13 states) $G_r(s)$.

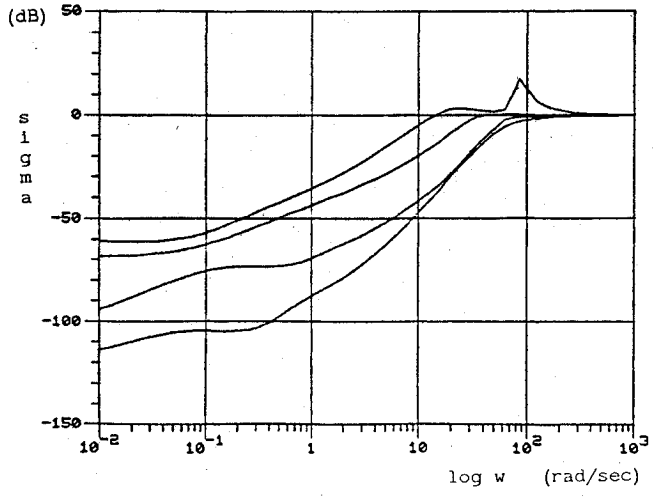

Fig. 3 Singular values of the multiplicative error transfer function matrix $E(j\omega)$ [Eq. (22] induced by the model reduction process.

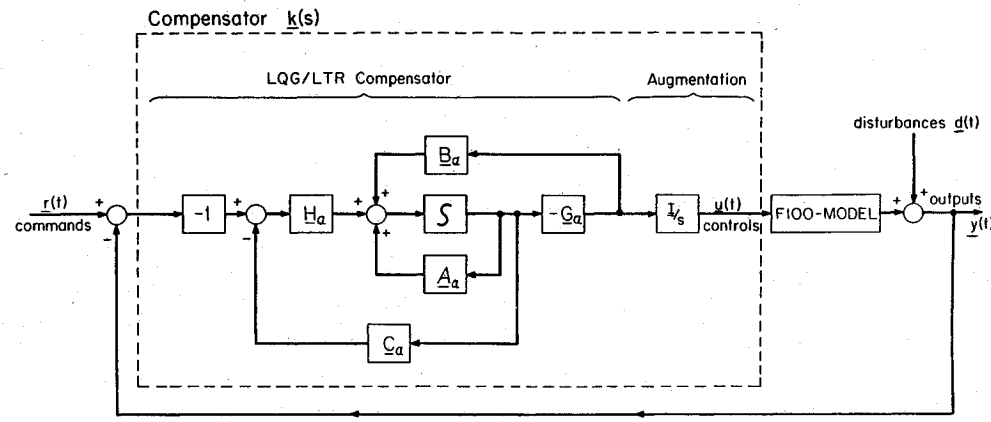

Fig. 4 Block diagram of the closed loop system resultant from the LQG/LTR design.

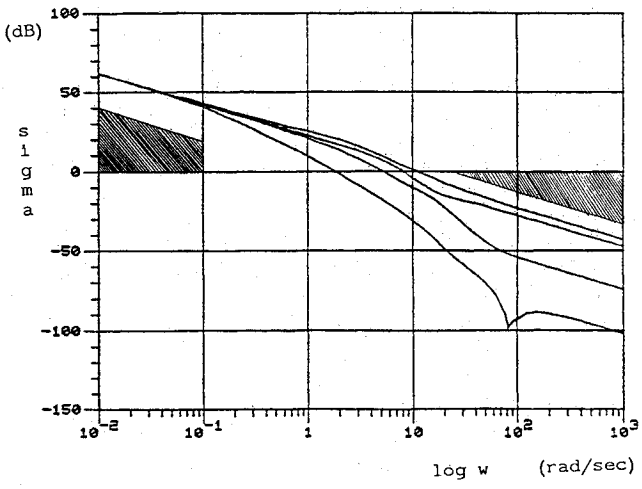

Fig. 5 Singular values of $G_{FOL}(j\omega)$, Eq. (28).

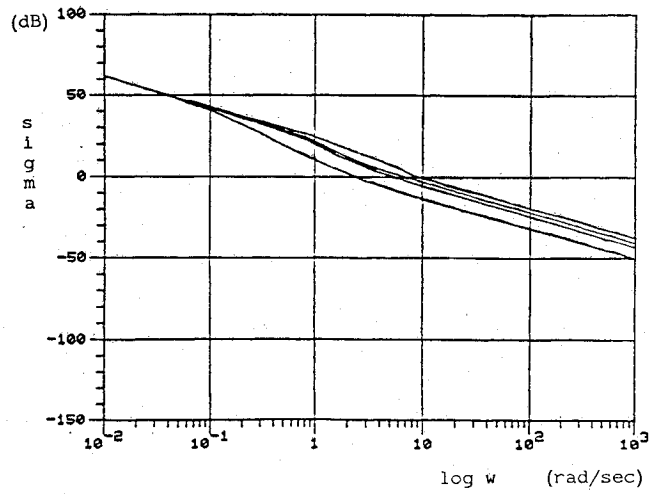

Fig. 6 Singular values of $G_{KF}(j\omega)$, Eq. (30). These singular values meet the performance and robustness specifications.

Eqs. (9) and (10) is

$$G_r(s) = H(sI-F)^{-1}G+D \tag{19}$$

and that

$$G_r(s) = \sum_{i=1}^{r} \frac{R_i/\lambda_i}{(s/\lambda_i)-1} + \sum_{i=r+1}^{n} \frac{R_i}{(-\lambda_i)} \tag{20}$$

Thus, the original model and the reduced model agree at *DC* ($s=0$).

5) Plot the singular values vs frequency of both the original and reduced systems. If the differences are significant go to step 1 and redefine the eigenvalue set to be retained.

Model Reduction for the F-100 Truth Model

Since the model reduction for the F-100 will be based on the magnitude of the residue matrices, it is necessary to scale (normalize) the variables of the full model. By the process of scaling, the physical units are eliminated and the magnitude of each residue matrix will better represent the importance of the corresponding pole. The F-100 linear model was scaled with the following output values: $N_1 = 100$ rpm, $N2 = 100$ rpm, $P_{t3} = 10$ psia, and $T_{t4.5} = 1°R$. The output scaling values were chosen so that the maximum singular values of the error $E(s) = [G(s) - G_r(s)]G_r^{-1}(s)$ is "nearly minimized,"

Table 5 shows the eigenvalues of the truth model and the corresponding ratios of the residue norms over the eigenvalue magnitude. Taking into consideration the specified crossover frequency of about 10 rad/s, we proceed as follows. The poles up to 12 rad/s will be retained due to their contribution to the low-frequency behavior *and* the "large" magnitude of their residue ratios. The poles at $-17.8 \pm j4.8$ and $-21 \pm j31.3$ have "large" residue ratios and they will also be retained. The rest of the poles, *either* because of small magnitude of their residue ratios (e.g., $\lambda_{12} = -18.59$ with residue ratio of 0.06) *or* because of their high frequency (e.g., $\lambda_{19} = -47.126$ with ratio 1.0037), are eliminated.

Following this step-by-step procedure for the model reduction, the 23 state "truth" model was reduced to a 13 state one.

Figure 2 shows the singular values of the scaled "truth" model and the singular values of the resultant reduced model. The reader should note that the singular values are virtually identical at low frequencies (up to about 10 rad/s). At high frequencies, the singular values of the reduced-order model flatten out. This is due to the fact that the reduced-order model has a nonzero D matrix [see Eqs. (10) (18)], so that in the reduced-order model the control $u(t)$ feeds through to the output $y(t)$ at high frequencies without the dynamic attenuation (roll-off) exhibited by the "truth" model.

Table 6 shows the open-loop poles and transmission zeros of the reduced-order model. The 13 poles in Table 6 are identical to those retained in the truth model (Table 4). However, the order reduction method changes the location and number of the transmission zeros. Comparison of Tables 4 and 6 reveals that the low-frequency zeros are relatively unaffected by the model reduction; however, the reduced-order model has several nonminimum phase zeros at frequencies about 10 rad/s that were not present in the "truth" model. These result from matching the phase shift without increasing the order of the reduced model. As is shown in the next section, where the use of the reduced-order model is outlined for the MIMO control synthesis, these nonminimum phase zeros do not present any problem in the use of the LQG/LTR methodology.

Table 5 Eigenvalues and residue matrix norms for truth model

Eigenvalue	$\|R_i\|/\|\lambda_i\|$	Eigenvalue	$\|R_i\|/\|\lambda_i\|$
1) -0.182	847.6	13) $-21+j31.3$	0.014
2) -0.648	350.3	14) $-21-j31.3$	0.014
3) -1.68	135.5	15)[a] $-21.3+j0.8$	0.035
4) -1.91	160.7	16)[a] $-21.3-j0.8$	0.035
5) -2.62	484.1	17)[a] -38.68	3.56
6) $-6.7+j1.3$	31.95	18)[a] -40	1.915
7) $-6.7-j1.3$	31.95	19)[a] -47.13	1.0037
8) -10	0.047	20)[a] -50.67	0.176
9) -12	1.84	21)[a] -59.2	0.33
10) $-17.8+j4.8$	0.489	22)[a] -175.7	0.005
11) $-17.8-j4.8$	0.489	23)[a] -577.0	3.24×10^{-6}
12)[a] -18.6	0.06		

[a]These poles were eliminated in the generation of the reduced-order model.

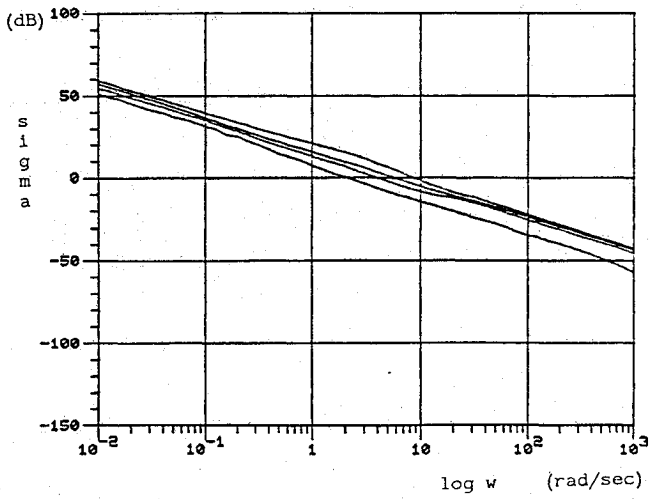

Fig. 7 Singular values of the LQG/LTR; $T_a(j\omega)$, Eq. (36). The engine model is the reduced one.

We can visualize the impact of the "modeling errors" between the F-100 "truth" and reduced-order models in the frequency domain, by the so-called[15,16] multiplicative error reflected at the plant output. Let $G(s)$ denote the transfer matrix of the 23 state "truth" model and let $G_r(s)$ denote that of the 13 state model. Then, let

$$G(s) \triangleq L(s)G_r(s) \triangleq [1+E(s)]G_r(s) \tag{21}$$

The multiplicative error $E(s)$ is then given by

$$E(s) = L(s) - I = [G(s) - G_r(s)]G_r^{-1}(s) \tag{22}$$

Figure 3 shows the singular values of $E(j\omega)$ vs frequency. As expected, the "worst" error, as quantified by $\sigma_{\max} E(j\omega)$ is small at low frequencies and becomes significant (greater than or equal to 1 or 0 dB) at about 12 rad/s. This behavior is to be expected by the very way we constructed the reduced-order model of the F-100 and is consistent with the bandwidth requirement. The robustness tests that utilize $\sigma_{\max} E(j\omega)$ will be discussed in the next section.

LQG/LTR Compensator Design

In this section, an LQG/LTR compensator will be designed for the reduced model $G_r(s)$ of the F-100 engine so that the closed-loop system will meet the posed specifications. This compensator will also be designed to be robust, such that it will stabilize the closed-loop system with the truth F-100 model.

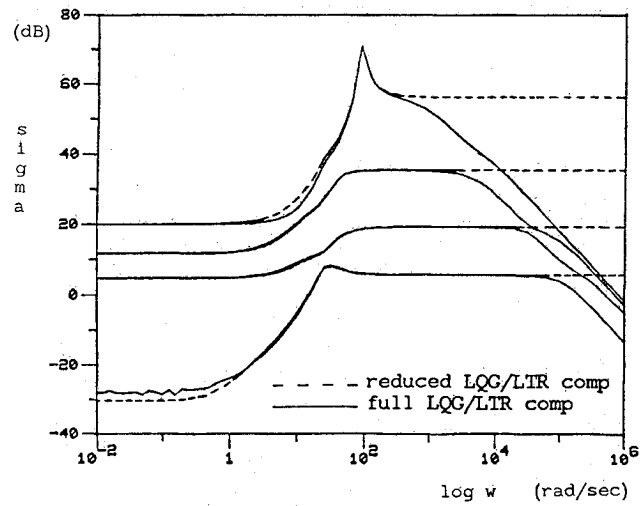

Fig. 8 Singular values of the LQG/LTR compensator $K_{LQG/LTR}(j\omega)$, Eq. (33), and singular values of the reduced order compensator $K_R(j\omega)$. Note the MIMO "phase lead" at crossover is preserved.

Since in the specifications a zero steady-state error for step commands and disturbances is required and since the engine model has no integrators, the plant $G_r(s)$ was augmented with four integrators one in each control channel. Figure 4 shows the closed-loop configuration using the reduced system $G_r(s)$, the augmentation I/s, and the LQG/LTR compensator for the augmented system. Thus, the overall compensator is $K(s) = (I/s)\,K_{LQG/LTR}(s)$.

Define

$$G_a(s) = G_r(s)\,(I/s)$$

to be the augmented system consisting of the reduced-order model and the integrators. The state-space representation of $G_a(s)$ can be written as

$$\dot{x}_a(t) = A_a x_a(t) + B_a u_a(t) \tag{23}$$

$$y(t) = C_a x_a(t)$$

$$G_a(s) = C_a(sI - A_a)^{-1}B_a \tag{24}$$

where

$$x_a^T = (\underbrace{x_1,\ldots,x_4}_{\text{integrator states}}, \underbrace{x_5,\ldots,x_{17}}_{\text{F-100 reduced states}})$$

$$A_a = \begin{bmatrix} 0 & 0 \\ G & F \end{bmatrix}, \quad B_a = \begin{bmatrix} I \\ 0 \end{bmatrix}, \quad C_a = [DH] \tag{25}$$

Table 6 Poles and zeros of the reduced model

Poles	Zeros
1) -0.182	1) 39.0
2) -0.648	2) 24.1
3) -1.68	3) $14.6+j17$
4) -1.91	4) $14.6-j17$
5) -2.62	5) $4.32+j88.0$
6) $-6.7+j1.3$	6) $4.32-j88.0$
7) $-6.7-j1.3$	7) -0.47
8) -10	8) -0.649
9) -12	9) -2.13
10) $-17.8+j4.8$	10) -19.47
11) $-17.8-j4.8$	11) $-20.4+j3.1$
12) $-21.3+j.8$	12) $-20.4-j3.1$
13) $-21.3-j.8$	

and the $[F,G,H,D]$ matrices are those of the reduced model.

Now, the step-by-step LQG/LTR[11-14] design procedure will be followed to find the compensator $K_{\text{LQG/LTR}}(s)$ for the augmented system $G_a(s)$.

Step 1. This step begins with the dynamics of the augmented system [Eqs. (23) and (24)] in order to find a scalar $\mu>0$ and a constant matrix L such that the singular values of the 4×4 matrix

$$G_{\text{FOL}}(s)=(1/\sqrt{\mu})G(sI-A_a)^{-1}L \tag{26}$$

"approximately" meet the specifications. In this study, we selected L so that at low frequencies ($s=j\omega\to0$) all singular values of $G_{\text{FOL}}(j\omega)$ are approximately the same; this will (eventually) cause all loops of the closed-loop system to behave in roughly the same way (in the sense of low-frequency command following and disturbance rejection). Once L is selected, then μ is adjusted (it acts as a gain parameter) to yield the desired crossover frequency of $\sigma_{\max}G_{\text{FOL}}(j\omega)$, which corresponds to the bandwidth of the fastest loop (about 10 rad/s).

The choice of L that causes the singular values of $G_{\text{FOL}}(j\omega)$ to be approximately the same at low frequencies is

$$L=\begin{bmatrix} G_r^{-1}(0) \\ \mathbf{0} \end{bmatrix} \tag{27}$$

where $G_r^{-1}(0)$ is the reduced-transfer matrix [Eq. (19)] at $s=0$. Substituting Eq. (27) into Eq. (26), we find

$$G_{\text{FOL}}(s)=\frac{1}{\sqrt{\mu}}\frac{I}{s}[H(sI-F)^{-1}G+D]G_r^{-1}(0) \tag{28}$$

so that at low fequencies ($s\to0$)

$$G_{\text{FOL}}(0)\cong\frac{I}{s}\cdot\frac{1}{\sqrt{\mu}} \tag{29}$$

Figure 5 shows the singular values $\sigma_i[G_{\text{FOL}}(j\omega)]$ calculated with $\mu=6\times10^{-3}$. Note in Fig. 5 that at low frequencies all of the singular values have a slope of -20 dB/dec and that the maximum crossover frequency is about 10 rad/s. The numerical values of L and μ are saved for subsequent calculations.

Step 2. In this step, we construct and analyze another 4×4 transfer function matrix $G_{KF}(s)$. In the LQG/LTR procedure,[11-14] $G_{KF}(s)$ is designed using Kalman filter concepts. The structure of $G_{KF}(s)$ is

$$G_{KF}(s)=C(sI-A_a)^{-1}H_a \tag{30}$$

where C_a and A_a are those defined by the augmented system of Eqs. (23-25) and H_a corresponds to the Kalman filter gain matrix.

To calculate the numerical value of the filter gain matrix H_a, one first solves the Kalman filter algebraic Riccati equation

$$A_a\Sigma+\Sigma A_a^T+LL^T-(1/\mu)\Sigma C_a^TC_a\Sigma=0 \tag{31}$$

using the numerical values of L and μ found in step 1 and then calculating the covariance matrix Σ. The filter gain matrix H_a is then computed from

$$H_a=(1/\mu)\Sigma C_a^T \tag{32}$$

Figure 6 shows the resultant singular values $\sigma_i[G_{KF}(j\omega)]$ for the F-100 model. Note that the crossover frequencies are between 2.5 and 9.0 rad/s and that at low frequency they decrease with a slope of -20 dB/s. They also meet the robustness constraint.

Step 3. The general structure of the LQG/LTR compensator $K_{\text{LQG/LTR}}(s)$ as shown in Fig. 4 is defined by the transfer function matrix[11-14]

$$K_{\text{LQG/LTR}}(s)=G_a(sI-A_a+B_aG_a+H_aC_a)^{-1}H_a \tag{33}$$

The matrices A_a, B_a, and C_a are those of the augmented system [Eqs. (23-25)]. The filter gain matrix H_a is that found in step 2 [see Eq. (32)]. The control gain matrix G_a in Eq. (33) is calculated by solving a "cheap-control" LQR problem, as described below.

First, one solves the following algebraic Riccati equation associated with the LQR problem:

$$KA_a+A_a^TK+qC_a^TC_a-KB_aB_a^TK=0 \tag{34}$$

for $q\to\infty$ (sufficiently large). In the F-100 engine design, the numerical value of q used was $q=10^{10}$. Then, one calculates the control gain matrix G_a according to

$$G_a=B_a^TK \tag{35}$$

The numerical value of the matrix G_a completes the specification of the LQG/LTR compensator transfer function $K_{\text{LQG/LTR}}(s)$ given by Eq. (33).

As $q\to\infty$, the LQG/LTR method guarantees that in the absence of nonminimum-phase zeros, pointwise in s, is

$$T_a(s)=G_a(s)K_{\text{LQG/LTR}}(s)\to G_{KF}(s) \tag{36}$$

Since the LTFM $G_{KF}(s)$ designed in step 2 meets the specifications, the approximation of Eq. (36) guarantees that the LQG/LTR design of Fig. 4 will also meet the specifications.

The singular values $\sigma_i[G_a(j\omega)\times K_{\text{LQG/LTR}}(j\omega)]$ for the F-100 design are shown in Fig. 7. Comparison of Figs. 6 and 7 shows that below 10 rad/s the approximation of Eq. (36) is excellent, in spite the presence of the nonminimum phase zeros (see Table 6). The reason that the nonminimum phase zeros did not influence the loop-transfer recovery process is due to the fact that the frequencies of the nonminimum phase zeros are beyond the frequency crossover region (2-10 rad/s).

Table 7 Eigenvalues and residue matrix magnitudes for $\bar{K}_{\text{LQG/LTR}}(s)$

Eigenvalues	$\|R_i\|/\|\lambda_i\|$	Eigenvalues	$\|R_i\|/\|\lambda_i\|$
1)[a] -0.47	2.24×10^{-2}	9) $-20.39+j3.12$	10.2
2)[a] -0.649	1.19×10^{-2}	10) $-20.39-j3.12$	10.2
3)[a] -2.13	4.19×10^{-3}	11) -21.2	0.448
4) $-6.39+j87.8$	368.4	12) -40.96	145.8
5) $-6.39-j87.8$	368.4	13) -56.72	328.6
6) $-12.8+j87.9$	99.65	14)[a] -764.8	825.0
7) $-12.0-j25.9$	99.65	15)[a] -7.77×10^{3}	118.8
8) -19.5	3.43	16)[a] -7.71×10^{4}	12.67
		17)[a] -2.5×10^{5}	3.07

[a]These eigenvalues were eliminated in the definition of the reduced-order compensator $K_R(s)$.

Figure 8 shows the singular values of the 4×4 compensator $K_{LQG/LTR}(s)$. It can be thought of as a MIMO "lead-lag" network that adds multivariable phase lead in the crossover frequency range to obtain the nice frequency domain "shapes" of Fig. 7. From an intuitive point of view, what the LQG/LTR compensator does is to create an approximate low-frequency inverse of the plant $G_a(s)$ and substitute the dynamics of $G_{KF}(s)$ to meet the specifications.

Note that, as $q\to\infty$ in the recovery process, the poles corresponding to the lags (high-frequency poles) of the compensator move to higher frequencies. This affects *only* the compensator $K(s)$; but, the $[G(s)K(s)]$ transfer matrix still meets the posed specifications. One could check the $[K(s)G(s)]$ transfer matrix, which depends on the assigned specifications and the condition number of $G(s)$. If $[K(s)G(s)]$ has undesirable loop shapes, one should change the specifications accordingly.

Step. 4. The LQG/LTR compensator was based upon the reduced 13-state model of the F-100. It is important to guarantee that when this compensator is used in conjunction with the 23-state "truth" model of the F-100, the closed-loop system remains stable. Such a stability-robustness check can be accomplished by checking, in the frequency domain, the inequality of Eq. (37), which involves the LTFM $T_a(s)$ [Eq. (36)] and the error matrix $E(s)$ [Eq. (22)], induced by the model-reduction approximation. Stability robustness can be guaranteed,[15,16] provided that the following singular value inequality holds for all frequencies ω:

$$\sigma_{\min}[I+T_a^{-1}(j\omega)]>\sigma_{\max}[E(j\omega)] \tag{37}$$

The singular values of the 4×4 matrices $I+T_a^{-1}(j\omega)$ and $E(j\omega)$ are shown in Fig. 9. It can be seen that Eq. (37) holds, so the compensator can be used with confidence to control the "truth" model of the F-100.

Since the truth model itself is an approximation of the real system and the small margin shown in Fig. 9 may be unacceptable, one could reduce the bandwidth (crossover) of the system to increase that margin. Also, one could include more poles in the reduced system to make the reduced model more accurate.

Step 5. In our problem, we can examine the use of $K_{LQG/LTR}(\omega)$, together with the appended integrators, in conjunction with the full 23-state "truth" model of the F-100. Figure 10 shows the singular values of the LTFM when the 23-state model is used. By comparing Figs. 7 and 10, we conclude that there is no significant change in stability, performance, and crossover behavior. Only the high-frequency characteristics are different, which has no effect on the system behavior.

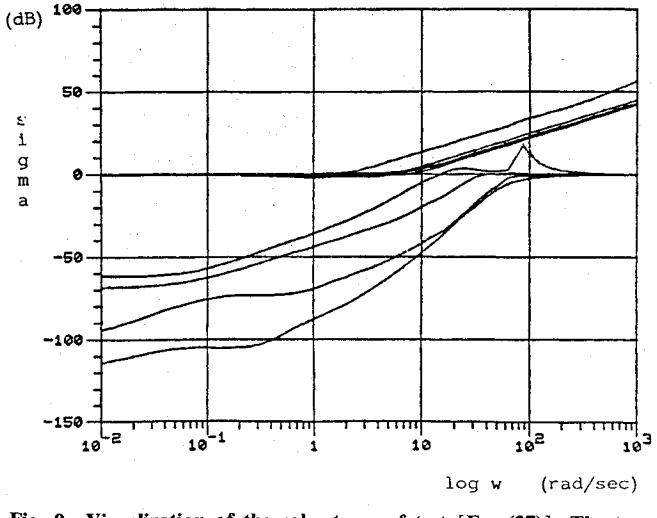

Fig. 9 Visualization of the robustness of test [Eq. (37)]. The top four curves are the singular values of $I+T_a^{-1}(j\omega)$, while the bottom four curves are the singular values of $E(j\omega)$.

Simplification of the LQG/LTR Compensator

A "possible" objection to LQG-based design is the high dimensionality of the resultant compensator for high-order systems. In this section, we demonstrate how one can use common sense and the residue method to reduce the order of the compensator $k_{LQG/LTR}(s)$ without any significant change in the performance and robustness properties of the closed-loop system.

Since the order of the augmented plant $G_a(s)$ was 17 (13 engine states plus the 4 "free" integrator states), the order of $K_{LQG/LTR}(s)$ is also 17. We can expand the 4×4 compensator transfer function matrix in a residue sum, similar to that of Eq. (6). Table 7 shows the 17 LQG/LTR compensator eigenvalues (poles) and the size of the corresponding magnitudes of $\|R_i/\lambda_i\|$. Following the residue method for model reduction, it was very easy to design a tenth-order reduced compensator with a 4×4 transfer function matrix denoted by $K_R(s)$—poles 4-13 in Table 7 whose singular values were identical to those $K_{LQG/LTR}(s)$ at DC ($s=0$).

Figure 8 shows the singular values of $K_R(j\omega)$ and the singular values of $K_{LQG/LTR}(j\omega)$. In Fig. 8, one can see that the reduced compensator $K_R(s)$ provides the necessary lead at the appropriate frequency range and, as such, it provides a

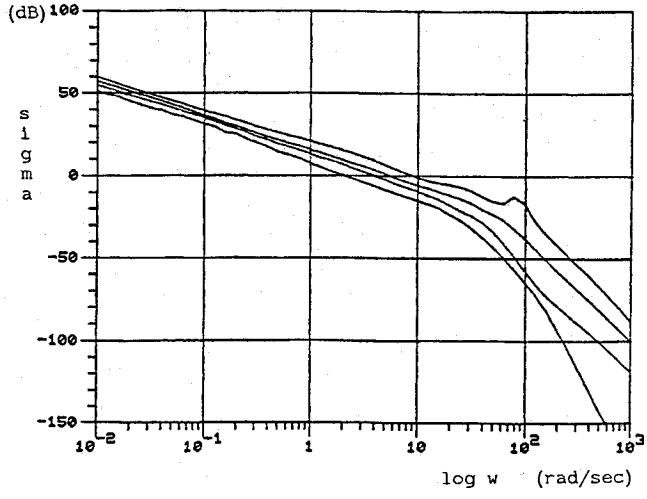

Fig. 10 Singular values of $G(j\omega)\cdot(I/j\omega)K_{LQG/LTR}(j\omega)$, where $G(j\omega)$ is the truth F-100 model (23 states). Compare with Fig. 7.

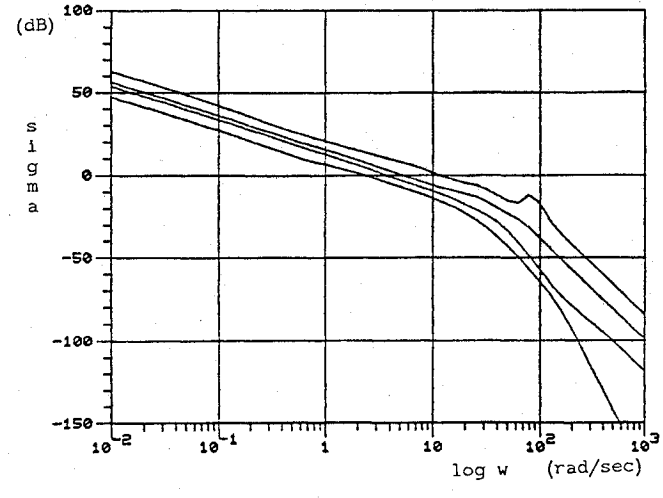

Fig. 11 Singular values of final LTFM using the reduced-order compensator and the truth model of the F-100. Compare with Fig. 10.

good approximation to $K_{LQG/LTR}(s)$ in the corresponding frequency range. The robustness check can be shown to be satisfied.

The bottom line, of course, is to demonstrate that the use of the reduced-order compensator together with the "free" integrators and the *truth* F-100 model $G(s)$ (23 states) meets the specifications. The resultant 4×4 LTFM, $T_R(s)$, is given by

$$T_R(s) = G(s) \cdot (I/s) \cdot K_R(s) \tag{38}$$

The singular values of $T_R(j\omega)$ are plotted in Fig. 11; note that the resultant crossover region is 2.5-11 rad/s. Comparison of Figs. 10 and 11 shows minor degradation in performance resulting from the use of $K_R(s)$ rather than the fully-blown LQG/LTR compensator. Of course, closed-loop stability is maintained.

Conclusions

This paper has demonstrated the specific steps that must be followed so as to apply the linear-quadratic Gaussian with the loop-transfer recovery method to design a control system for the F-100 turbofan engine. We have stressed the integration of frequency-domain and time-domain state-space ideas inherent in the linear-quadratic Gaussian with the loop-transfer recovery method. We emphasized that the design process involves several approximation phases and that model and compensator simplifications should not be carried out in a vacuum; rather, such simplifications should be carried out in concert with the proposed performance and robustness specifications.

Acknowledgment

The authors are grateful to Dr. Gunter Stein for his numerous discussions and suggestions that have contributed to making modern control theory practical. Research was supported by the General Electric Corporate Research and Development Center and by NASA Ames and Langley Research Centers under Grant NASA/NAG 2-297.

References

[1]Sain, M.K. et al. (eds), *Alternative for Linear Multivariable Control,* National Engineering Consortium, Chicago, 1978.

[2]DeHoff, R.L., et al., "F-100 Multivariable Control Synthesis Program," Vol. I, AFAPL TR-77-35, 1976.

[3]Miller, R.J. and Hackney, R.D., "F-100 Multivariable Control System Engine Models/Design Criteria," AFAPL TR-76-74, 1976.

[4]Szuch et al., "F-100 Multivariable Control Synthesis Program-Evaluation of a Multivariable Control Using a Real-Time Engine Simulation," NASA TP 1056, 1977.

[5]Kappos, E., "Robust Multivariable Control for the F-100 Engine," S.M. Thesis (LIDS-TH-1328), Massachusetts Institute of Technology, Cambridge, Sept. 1983.

[6]Idelchick, M., "An Application of Modern Control Theory to a High-Bypass Variable Compressor Geometry Engine," S.M. Thesis (LIDS-TH-1127), Massachusetts Institute of Technology, Cambridge, July 1981.

[7]Kapasouris, P., "Gain-Scheduled Multivariable Control for the GE-21 Turbofan Engine Using the LQR and LQG/LTR Methodologies," S.M. Thesis (LIDS-TH-1380), Massachusetts Institute of Technology, Cambridge, May 1984.

[8]Pfeil, W., "Multivariable Control for the GE T700 Engine Using the LQG/LTR Methodology," S.M. Thesis, Massachusetts Institute of Technology, Cambridge, June 1984.

[9]Athans, M., "The Role and Use of the LQG Problem in Control System Design," *IEEE Transactions on Auto. Control,* Vol. AC-16, Dec. 1971, pp. 529-552.

[10]Kwakernaak, H., and Sivan, R., *Linear Optimal Control Systems,* John Wiley & Sons, New York, 1972.

[11]Doyle, J.C. and Stein G., "Multivariable Feedback Design: Concepts for a Classical Modern Synthesis," *IEEE Transactions on Auto. Control,* Vol. AC-26, Feb. 1981, pp. 4-16.

[12]Stein, G., "LQG-Based Multivariable Design Frequency Domain Interpretation," AGARD-LS-117 NATO, 1981.

[13]Stein, G. and Athans, M., "The LQG-LTR Procedure for Multivariable Feedback Control Design," Rept. LIDS-R-1384, Massachusetts Institute of Technology, Cambridge.

[14]Athans, M., "Lecture Notes on Multivariable Control Systems: MIT Subject 6.232," Massachusetts Institute of Technology, Cambridge, 1984.

[15]Lehtomaki, N.A., "Practical Robustness Measures in Multivariable Control System Analysis," Ph.D. Thesis (LIDS-TH-1093), Massachusetts Institute of Technology, Cambridge, May 1981.

[16]Lehtomaki, N.A., Sandell Jr., N.R., and Athans, M., "Robustness Results in LQG-Based Multivariable Control Design," *IEEE Transactions on Automatic Control,* Vol. AC-26, Feb. 1981, pp. 75-92.